Oscillation of satellite droplets in an Oldroyd-B viscoelastic liquid jet

Fang Li,* Xie-Yuan Yin, and Xie-Zhen Yin
Department of Modern Mechanics, University of Science and Technology of China, Hefei, Anhui 230027, People's Republic of China
(Received 8 June 2016; published 31 January 2017)

A one-dimensional numerical simulation is carried out to study the oscillation characteristics of satellite droplets in the beads-on-a-string structure of an Oldroyd-B viscoelastic liquid jet. The oscillation of satellite droplets is compared with the linear oscillation of a single viscoelastic droplet. It is found that, contrary to the predictions of linear theory, the period of oscillation of satellite droplets decreases with time, despite the increase in droplet volume. The mechanism may lie in the existence of the filament, which exerts an extra resistance on droplets. On the other hand, the oscillation of droplets does not influence very much the thinning of the filament. The influence of the axial wave number, viscosity, and elasticity on the oscillation of satellite droplets is examined. Increasing the wave number may result in the decrease in the period and the increase in the decay rate of oscillation, while increasing viscosity may lead to the increase in both the period and the decay rate of oscillation. Elasticity is shown to suppress the oscillation at large wave numbers, but its influence is limited at small wave numbers.

DOI: 10.1103/PhysRevFluids.2.013602

I. INTRODUCTION

Instability and breakup of viscoelastic liquid jets is a fundamental problem in applications such as inkjet printing, liquid bridges, atomization, fiber spinning, and coating. In the linear scope, instability of viscoelastic liquid jets has been well understood. Elasticity is known to enhance instability of viscoelastic jets, and viscoelastic jets are more unstable than their Newtonian counterparts [1–3]. For a purely viscoelastic liquid jet, the axisymmetric mode is more unstable than all nonaxisymmetric modes [4,5]. However, in the presence of a strong electric field or fast coflowing air, the first nonaxisymmetric mode may become dominant [6,7]. Both viscoelasticity and surface tension have a strong stabilizing or destabilizing influence on the instability of viscoelastic jets [1–5].

Nonlinear instability studies showed that breakup of viscoelastic jets can be greatly delayed by elasticity [8,9]. Several one-dimensional models have been established and used in numerical simulations [10–13]. These one-dimensional models greatly save computation time and captured well the nonlinear characteristics of viscoelastic jets. The dynamics in droplet migration, droplet oscillation, droplet merging, and droplet drainage was revealed by Li and Fontelos [11], and the thinning of the filament was investigated by Ardekani *et al.* [12], Renardy [14], and Entov and Hinch [15]. In the highly axially stretched state, the filament thins exponentially at a rate $1/3\mathrm{De}$, the extension rate in the filament remains $2/3\mathrm{De}$, and the polymer stress in the filament increases exponentially at a rate $1/3\mathrm{De}$, where De is the Deborah number. The self-similar problem at the corner joining the filament to the droplet was solved by Clasen *et al.* [10] and Bhat *et al.* [13]. Sattler *et al.* [16] and Eggers [17] studied, experimentally and theoretically, the final stages of capillary breakup of semidilute polymer solutions. They found that highly stretched threads become unstable and form a nonuniform "blistering" pattern (blistering instability), being different generations of tiny drops separated by threads of highly concentrated polymer solution.

For a viscoelastic jet, at small wave numbers or low viscosities, a beads-on-a-string structure with satellite droplets is eventually formed. However, at large wave numbers or high viscosities, no

*fli6@ustc.edu.cn

satellite droplet exists in the structure [12]. Moreover, at small viscosities, both main and satellite droplets oscillate around their equilibrium positions due to the interplay of capillary and inertial forces. Although the dynamics in a beads-on-a-string structure has been extensively explored, little attention has been paid to the oscillation of droplets, which motivates the present work.

The paper is organized as follows. In Sec. II the one-dimensional viscoelastic model is described. In Sec. III the numerical results are presented and discussed. A brief linear instability study of the viscoelastic jet is carried out; the oscillation characteristics of satellite droplets in beads-on-a-string structures are highlighted; and the effects of the axial wave number, viscosity, and elasticity on the oscillation are investigated. In Sec. IV main conclusions are drawn.

II. ONE-DIMENSIONAL VISCOELASTIC MODEL

Consider an infinitely long cylindrical liquid jet of radius R and axial velocity U. For convenience, a relative coordinate system (r,θ,z) moving together with the jet is utilized to describe the problem, where r, θ, and z are the radial, azimuthal, and axial coordinates, respectively. The liquid is a dilute polymer solution of density ρ. The viscoelasticity of the liquid is described by the Oldroyd-B constitutive equation [18]. The medium surrounding the jet is air; the hydrodynamic effect of the air is neglected. The governing equations are the continuity equation, the momentum equation, and the constitutive equation:

$$\nabla \cdot \boldsymbol{v} = 0, \tag{1}$$

$$\rho\left(\frac{\partial \boldsymbol{v}}{\partial t} + \boldsymbol{v}\cdot\nabla\boldsymbol{v}\right) = -\nabla p + \eta_s\nabla^2\boldsymbol{v} + \nabla\cdot\tau_p, \tag{2}$$

$$\tau_p + \lambda\left[\frac{\partial \tau_p}{\partial t} + \boldsymbol{v}\cdot\nabla\tau_p - (\nabla\boldsymbol{v})^T\cdot\tau_p - \tau_p\cdot\nabla\boldsymbol{v}\right] = 2\eta_p\boldsymbol{D}, \tag{3}$$

where $\boldsymbol{v}$ is the velocity vector, p is the pressure, η_s is the viscosity of the solvent, τ_p is the polymer stress tensor, λ is the stress relaxation time, η_p is the viscosity of the polymer, the superscript T denotes the transpose, and $\boldsymbol{D} = {}^1\!/_2[\nabla\boldsymbol{v} + (\nabla\boldsymbol{v})^T]$ is the rate-of-strain tensor. At the jet surface, the kinematic and dynamic boundary conditions must be satisfied:

$$\frac{dF}{dt} = 0, \tag{4}$$

$$p\boldsymbol{n} - 2\eta_s\boldsymbol{D}\cdot\boldsymbol{n} - \tau_p\cdot\boldsymbol{n} = \sigma\nabla\cdot\boldsymbol{n}\boldsymbol{n}, \tag{5}$$

where $F = r - h(z,t) = 0$ is the surface function being h the radius of the perturbed jet, d/dt is the material derivative, $\boldsymbol{n}$ is the outward unit vector normal to the surface, and σ is the surface tension coefficient.

Suppose that the jet is perturbed by a long-wavelength axisymmetric disturbance. The slender-body approximation can be applied [8,19]. By choosing the radius of the jet R, the capillary time $\tau_c = \sqrt{\rho R^3/\sigma}$ and the capillary force σ/R as scales of length, time, and pressure, respectively, the governing equations and boundary conditions (1)–(5) yield the following nondimensionalized one-dimensional equations [10–12]:

$$\frac{\partial h}{\partial t} + u\frac{\partial h}{\partial z} = -\frac{h}{2}\frac{\partial u}{\partial z}, \tag{6}$$

$$\frac{\partial u}{\partial t} + u\frac{\partial u}{\partial z} = -\frac{\partial}{\partial z}(\nabla\cdot\boldsymbol{n}) + 3\beta\mathrm{Oh}\frac{1}{h^2}\frac{\partial}{\partial z}\left(h^2\frac{\partial u}{\partial z}\right) + \frac{1}{h^2}\frac{\partial}{\partial z}[h^2(\tau_{zz} - \tau_{rr})], \tag{7}$$

$$\nabla\cdot\boldsymbol{n} = \frac{1}{[1 + (\partial h/\partial z)^2]^{3/2}}\left[\frac{1 + (\partial h/\partial z)^2}{h} - \frac{\partial^2 h}{\partial z^2}\right], \tag{8}$$

$$\tau_{zz} + \mathrm{De}\left(\frac{\partial \tau_{zz}}{\partial t} + u\frac{\partial \tau_{zz}}{\partial z} - 2\tau_{zz}\frac{\partial u}{\partial z}\right) = 2(1-\beta)\mathrm{Oh}\frac{\partial u}{\partial z}, \tag{9}$$

$$\tau_{rr} + \mathrm{De}\left(\frac{\partial \tau_{rr}}{\partial t} + u\frac{\partial \tau_{rr}}{\partial z} + \tau_{rr}\frac{\partial u}{\partial z}\right) = -(1-\beta)\mathrm{Oh}\frac{\partial u}{\partial z}, \tag{10}$$

where u is the axial velocity component, and τ_{zz} and τ_{rr} are the zz and rr components of the polymer stress tensor. The relevant dimensionless parameters are the Ohnesorge number $\mathrm{Oh} = \eta_0/\sqrt{\rho\sigma R}$, where $\eta_0 = \eta_s + \eta_p$ is the zero-shear viscosity of the solution, the Deborah number $\mathrm{De} = \lambda/\tau_c$, and the solvent to solution viscosity ratio $\beta = \eta_s/\eta_0$. The one-dimensional equations (6)–(10) are the same as those in Refs. [10–13]. In particular, (6) and (7) can be written in conservative form [10–12]:

$$\frac{\partial h^2}{\partial t} + \frac{\partial h^2 u}{\partial z} = 0, \tag{11}$$

$$\frac{\partial h^2 u}{\partial t} + \frac{\partial h^2 u^2}{\partial z} = \frac{\partial}{\partial z}\left[h^2\left(K + 3\beta\mathrm{Oh}\frac{\partial u}{\partial z} + \tau_{zz} - \tau_{rr}\right)\right], \tag{12}$$

where

$$K = \frac{1}{[1+(\partial h/\partial z)^2]^{3/2}}\left[\frac{1+(\partial h/\partial z)^2}{h} + \frac{\partial^2 h}{\partial z^2}\right]. \tag{13}$$

III. NUMERICAL RESULTS

The one-dimensional equations are solved by using an adaptive implicit finite difference method [20]. In order to guarantee the required accuracy that the maximum relative error of all quantities is below 0.1%, 1000 grids are used in space discretization, and the dimensionless time step is 5×10^{-4}. The code is verified by comparing with the result in Refs. [10,12]. Due to symmetry, only a half-wavelength segment of the jet is calculated. At two ends $z = 0$ and $z = \lambda/2$, where λ is the wavelength, the following periodic boundary conditions are imposed:

$$\frac{\partial h}{\partial z}(z=0,t) = \frac{\partial h}{\partial z}\left(z=\frac{\lambda}{2},t\right) = 0, \tag{14}$$

$$u(0,t) = u\left(\frac{\lambda}{2},t\right) = 0, \tag{15}$$

$$\frac{\partial \tau_{zz}}{\partial z}(0,t) = \frac{\partial \tau_{zz}}{\partial z}\left(\frac{\lambda}{2},t\right) = 0, \tag{16}$$

$$\frac{\partial \tau_{rr}}{\partial z}(0,t) = \frac{\partial \tau_{rr}}{\partial z}\left(\frac{\lambda}{2},t\right) = 0. \tag{17}$$

At the initial time, the surface of the jet is supposed to be perturbed by a cosine wave,

$$h(z,t=0) = \sqrt{1-\frac{\varepsilon_0^2}{2}} + \varepsilon_0\cos(kz), \tag{18}$$

where k is the axial wave number and ε_0 is the initial amplitude of the wave. In the calculation ε_0 is taken to be 0.05.

As to the physical properties of the liquid, we choose $\rho = 1000\,\mathrm{kg/m^3}$, $\eta_0 = 3.7\,\mathrm{mPa\,s}$, $\eta_s = 1\,\mathrm{mPa\,s}$, $\lambda = 0.17\,\mathrm{ms}$, and $\sigma = 0.06\,\mathrm{N/m}$, the same as in Ref. [12]. The radius of the jet is taken to be $140\,\mu\mathrm{m}$. As a result, the values of the dimensionless parameters are $\mathrm{Oh} = 0.04$, $\beta = 0.27$, and $\mathrm{De} = 0.8$, which are maintained unchanged in the calculation unless specified otherwise.

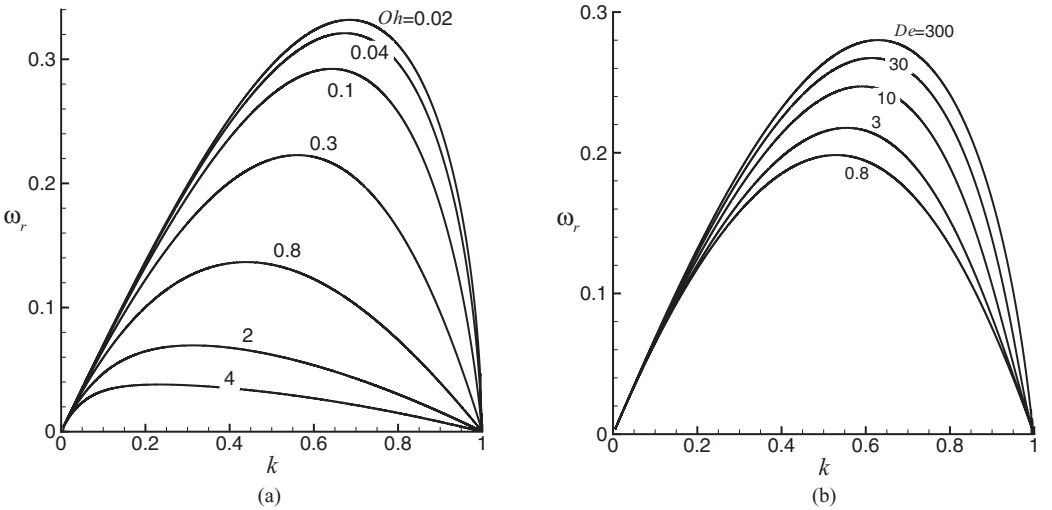

FIG. 1. The temporal growth rate ω_r versus the axial wave number k for (a) different values of Oh, De $= 0.8$, and (b) different values of De, Oh $= 0.4$. $\beta = 0.27$.

A. Linear instability study of the viscoelastic liquid jet

It is well known that linear theory can correctly describe the motion of a jet initially perturbed by a small disturbance [21,22]. Assume that the disturbance is of normal mode form $a\exp(\omega t + ikz)$, where a is the initial amplitude of the disturbance, ω is the complex frequency with the real part ω_r the temporal growth rate and the imaginary part ω_i the angular frequency, and i is the imaginary unit. Substitution of the normal mode into (1)–(5) and linearization yields a set of homogeneous equations. In order that the equations have nontrivial solutions, the determinant of the coefficient matrix must be equal to zero, which gives the following dispersion relation:

$$Q(k)k^{-2}\omega^2 + 2C^*\omega[2Q(k) - 1] + 4C^*k^2[Q(k) - Q(l)] - 1 + k^2 = 0, \tag{19}$$

where

$$l = \sqrt{k^2 + \frac{\omega}{C^*}}, \quad C^* = \mathrm{Oh}\frac{1 + \beta\omega De}{1 + \omega De}, \quad Q(x) = x\frac{I_0(x)}{I_1(x)},$$

where $I_n(x)$, $n = 0, 1$, is the nth-order modified Bessel functions of the first kind with respect to the argument x. The dispersion relation (19) is coincident with those in Refs. [1,23].

The effects of viscosity and elasticity on the instability of the viscoelastic jet are shown in Figs. 1(a) and 1(b), respectively. In Fig. 1(a), the temporal growth rate ω_r decreases as the Ohnesorge number increases, indicating that viscosity has a stabilizing effect on the instability of the jet. In Fig. 1(b) the growth rate increases as the Deborah number increases, indicating that elasticity has a destabilizing effect on the instability of the jet. Most intriguingly, neither viscosity nor elasticity influences the cut-off wave number, which is always equal to 1. That is, a viscoelastic jet is unstable for any disturbance of wavelength larger than the circumference of the jet, analogous to a viscous or inviscid jet [3,21]. Based on this fact, in the nonlinear study, the axial wave number should be smaller than 1.

B. Oscillation characteristics of satellite droplets

A typical profile of the beads-on-a-string structure with an oscillating satellite droplet between two adjacent main droplets is shown in Fig. 2(a), where the droplets are connected by a thin filament of axially uniform thickness. The time evolution of the radius of the jet at $z = \lambda/2$ (where the satellite droplet lies), denoted by $h_{\lambda/2}$, is shown in Fig. 2(b). As clearly seen from the figure, the

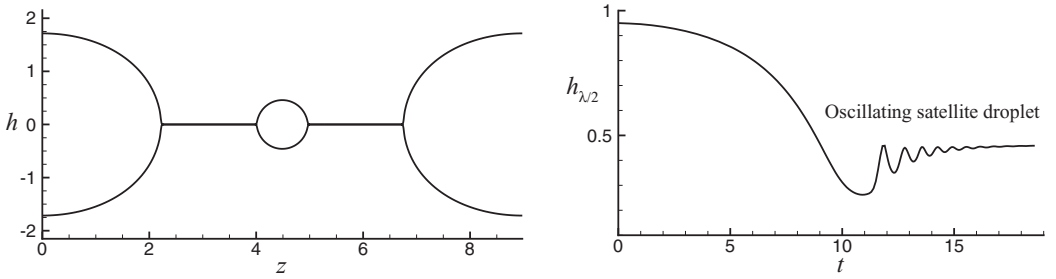

FIG. 2. (a) Typical profile of the beads-on-a-string structure with an oscillating satellite droplet between two adjacent main droplets. (b) The time variation of the radius of the jet at $z = \lambda/2$. $k = 0.7$, Oh $= 0.1$, De $= 0.8$, $\beta = 0.27$.

satellite droplet oscillates at large times. The oscillation is damped by viscosity and eventually dies out, resulting in an almost spherical shape of the satellite droplet.

It seems difficult to analyze the oscillation of the satellite droplet in the presence of the filament. Fortunately, its oscillation is analogous to the shape oscillation of a single viscoelastic drop of the fundamental mode $m = 2$ [12]. There have been some reports about oscillation of single viscoelastic drops in the literature [24–28]. Ardekani *et al.* [12] compared the periods of oscillation of satellite droplets estimated from the one-dimensional simulation with those predicted by linear theory of a single inviscid droplet. In the following, we will make a more accurate comparison by taking into account liquid viscoelasticity. Assume that the disturbance is small. In the spherical coordinate system (r,Θ,φ), where r, Θ, φ are the radius, azimuth angle, and polar angle, respectively, the perturbed surface of a single viscoelastic liquid droplet is

$$r = R_{\text{drop}}[1 + \varepsilon P_2(\cos\theta)\exp(-\alpha_2 t)], \tag{20}$$

where R_{drop} is the radius of the droplet normalized by the radius of the jet R, ε is a small value measuring the initial amplitude of the oscillation, $P_2(\cos\theta)$ is the Legendre polynomial of mode $m = 2$, and α_2 is the complex frequency being the real part α_r the decay rate and the imaginary part α_i the angular frequency. The governing equations and boundary conditions are (1)–(5), too. Introducing the small perturbation (20) and linearizing the equations leads to the following characteristic equation [26,27]:

$$\left(\frac{\alpha_{2,0}}{\alpha_2}\right)^2 = \frac{6}{q^2 - 2qW(q)} - 1 + \frac{4}{q^2}\left[1 + \frac{3W(q)}{W(q) - q/2}\right], \tag{21}$$

where

$$\alpha_{2,0} = 2\sqrt{2}R_{\text{drop}}^{-3/2}, \quad q = R_{\text{drop}}\sqrt{\frac{\alpha_2}{\text{Oh}}\frac{1-\alpha_2\text{De}}{1-\alpha_2\beta\text{De}}}, \quad W(q) = \frac{j_3(q)}{j_2(q)},$$

$j_n(q), n = 2,3$, is the nth-order spherical Bessel function of the first kind with respect to the argument q, and $\alpha_{2,0}$ is the angular frequency for an inviscid droplet [22]. The transcendental equation (21) is solved numerically. The validity of the code is checked by comparing with the result in Ref. [27].

The solution of (21) is shown in Fig. 3, for different values of k and Oh. It can be seen from the figure that the decay rate α_r is always positive, indicating that the perturbation is always damped. When the angular frequency α_i is nonzero, the droplet undergoes periodic oscillation. For example, for $k = 0.7$ and Oh $= 0.1$, α_i is nonzero, so the droplet oscillates periodically, in agreement with the result in Fig. 2.

The comparison between the one-dimensional numerical results and the predictions of linear theory is illustrated in Table I, where we show that the numerical results and the linear predictions

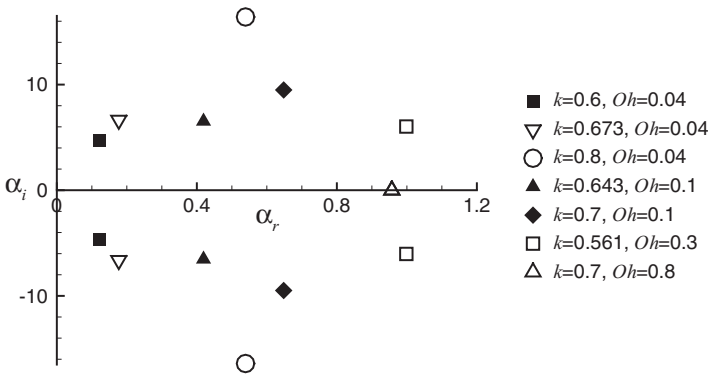

FIG. 3. The solution of the characteristic equation (21) on the complex α plane for different values of k and Oh. De $= 0.8$, $\beta = 0.27$.

are close to each other. The discrepancies between them may be caused by the fact that the radius of the satellite droplet R_{drop}, which is estimated from the one-dimensional simulation and is used to calculate the inviscid angular frequency $\alpha_{2,0}$ in Eq. (21), cannot be very accurate, because the volume of a satellite droplet changes all the time during the evolution of a beads-on-a-string structure [11,12]. In addition, the existence of the filament may have some influence on the oscillation of the satellite droplet.

As shown in Table I, both the axial wave number and the Ohnesorge number influence the oscillation of the satellite droplet. For a fixed Ohnesorge number, as k increases, the size of the satellite droplet R_{drop} decreases, the period of oscillation t_p decreases, and the decay rate α_r increases, indicating that increasing the axial wave number suppresses the oscillation of the satellite droplet. As Oh increases, the most unstable wave number $k_{\max}$ decreases, and R_{drop} increases together with t_p and α_r, indicating that viscosity suppresses the oscillation of the satellite droplet.

The suppression effect of viscosity on the oscillation of the satellite droplet can be observed by studying the time evolution of the radius of the jet; see Fig. 4. For a larger Oh, the initial amplitude of oscillation is smaller and the oscillation is damped more rapidly. When Oh is as large as 0.8, the oscillation becomes aperiodic. It is predicted that the oscillation will disappear as Oh increases further.

At a fixed axial wave number and a fixed Ohnesorge number, the period of oscillation of the satellite droplet is actually not a constant. The period of oscillation $t_{p,1D}$ collected in Table I comes from the first period of oscillation. The variation of the period of oscillation for a sequence of oscillation periods is shown in Fig. 5, where $k_{\max} = 0.643$ and Oh $= 0.1$. As seen in the figure, the period of oscillation is comparable to the capillary time, and it obviously decreases with time

TABLE I. Comparison between the oscillation period t_p and the decay rate α_r from the one-dimensional simulation (denoted by the subscript $1D$) and the predictions of linear theory (denoted by the subscript *linear*). The period of oscillation $t_{p,1D}$ comes from the first oscillation. De $= 0.8$, $\beta = 0.27$. The asterisk denotes the most unstable wave numbers predicted by linear theory.

k	Oh	R_{drop}	$t_{p,1D}$	$t_{p,\text{linear}}$	$\alpha_{r,1D}$	$\alpha_{r,\text{linear}}$
0.6	0.04	0.72	1.21	1.34	0.095	0.122
0.673*	0.04	0.57	0.91	0.947	0.13	0.177
0.8	0.04	0.31	0.35	0.382	0.50	0.539
0.643*	0.1	0.58	1.15	0.96	0.34	0.419
0.7	0.1	0.45	0.60	0.662	0.77	0.648
0.561*	0.3	0.62	1.12	1.04	1.29	1.0

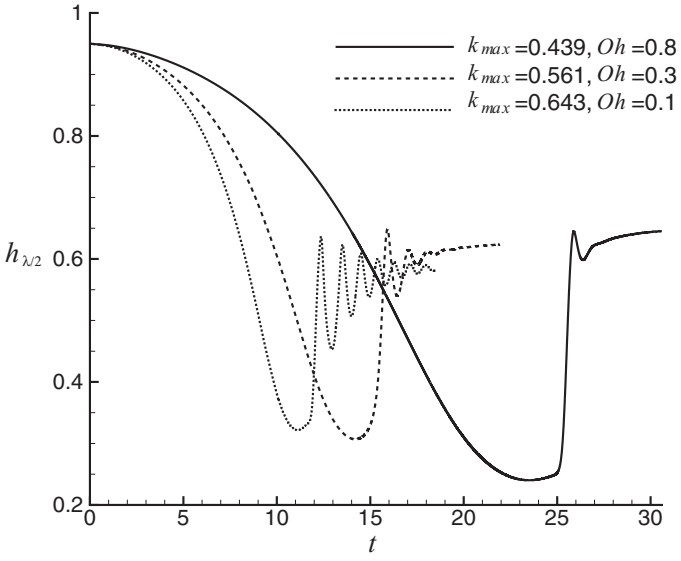

FIG. 4. The time evolution of the radius of the jet at $z = \lambda/2$ for the most unstable wave numbers at different values of Oh. De $= 0.8$, $\beta = 0.27$.

(see the long dashed line with empty squares). Meanwhile, the radius of the satellite droplet R_{drop} slightly increases with time due to liquid drainage in the filament (see the short dashed line with empty circles).

Consider the small-amplitude oscillation of an independent liquid droplet. If the liquid is inviscid, the period of oscillation of the droplet is $T_{\text{inviscid}} = \pi/\sqrt{2}R_{\text{drop}}^{3/2}$ [12,22], namely, the period of oscillation increases with the size of the droplet. If the liquid is Newtonian viscous, the period of oscillation is $T_{\text{viscous}} = T_{\text{inviscid}}/\sqrt{1-\zeta^2}$ with $\zeta = 2.5/\sqrt{2}\text{Oh}R_{\text{drop}}^{-1/2}$ [29,30], indicating that the period of oscillation increases with liquid viscosity, and when $\text{Oh} \geqslant 2\sqrt{2}/5R_{\text{drop}}^{1/2}$ the droplet no longer oscillates. Moreover, the increase in droplet size leads to the increase in the period of oscillation. If the liquid is Oldroyd-B viscoelastic, according to (21), the trends are the same as those for a viscous droplet. That is, linear

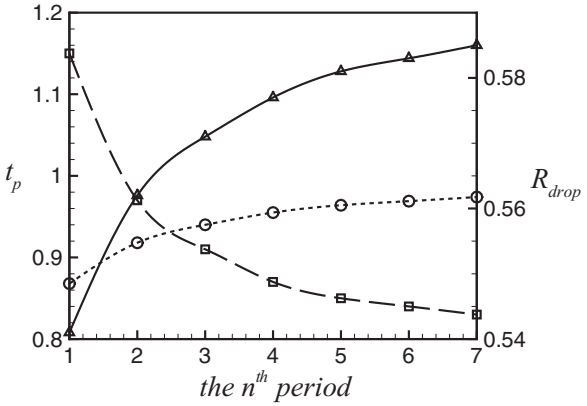

FIG. 5. The period of oscillation t_p for a sequence of oscillation periods (long dashed line with squares) for $k_{\text{max}} = 0.643$ at Oh $= 0.1$, estimated from the one-dimensional numerical simulation. The short dashed line with circles denotes the radius of the satellite droplet R_{drop}. The solid line with triangles denotes the period of oscillation t_p calculated from linear theory. De $= 0.8$, $\beta = 0.27$.

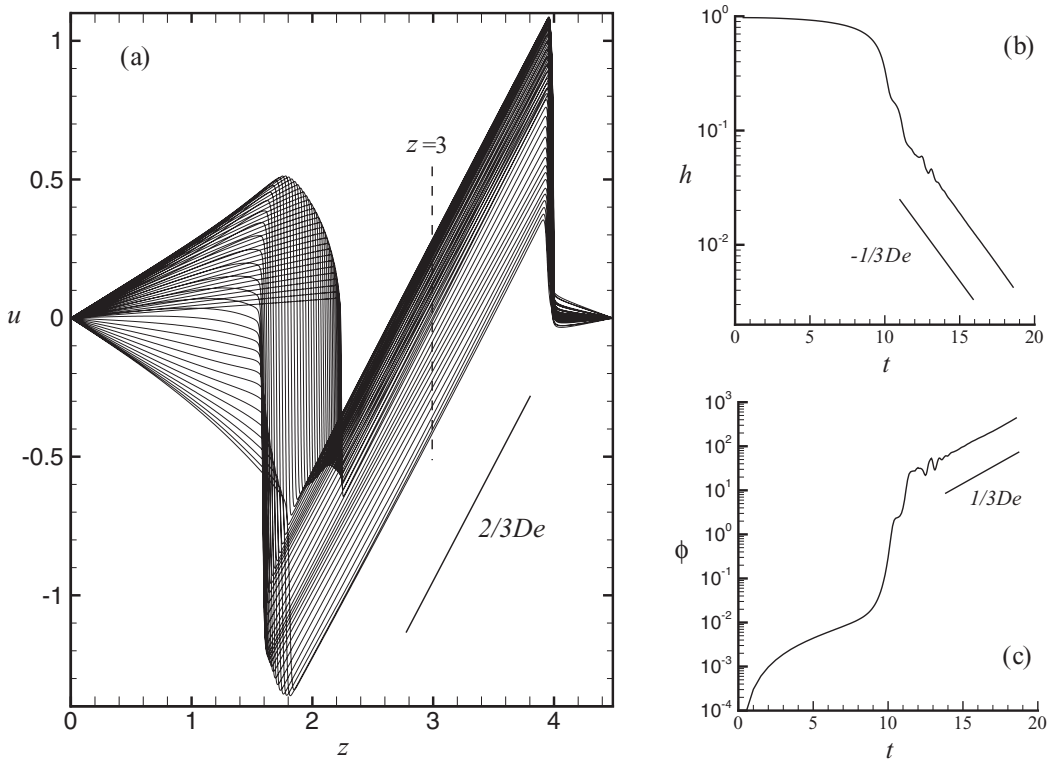

FIG. 6. (a) The profiles of the axial velocity u at different instants of time. (b) The time evolution of the radius of the jet at $z = 3$. (c) The time evolution of the first normal stress difference ϕ at $z = 3$. $k = 0.7$, $\mathrm{Oh} = 0.1$, $\mathrm{De} = 0.8$, $\beta = 0.27$.

theory predicts that the period of oscillation of a viscoelastic droplet increases as its size increases, as shown in Fig. 5 (see the solid line with empty triangles), in contrast with the one-dimensional simulation result.

It is natural to attribute the decrease in the period of oscillation of the satellite droplet to the existence of the filament. According to (12), the filament exerts an axial force $\pi h^2(K + 3\beta \mathrm{Oh}\frac{\partial u}{\partial z} + \tau_{zz} - \tau_{rr})$ on the satellite droplet at the two poles of it. Moreover, as the thickness of the filament decreases with time, this extra force increases. It possibly acts as a restoring force, suppressing the oscillation of the satellite droplet and inducing the decrease in its period.

The effect of the oscillation of the droplets on the thinning of the filament is shown in Fig. 6, where the values of the parameters are the same as in Fig. 2. As can be seen in Fig. 6(a), the axial velocity u in the filament varies with time, due to the oscillation of the main droplet (at $z = 0$) and the satellite droplet (at $z = 4.5$). In the middle part of the filament, the velocity changes its sign, indicating an oscillation of the liquid there. Differently, at the two ends of the filament, the axial velocity is always negative or positive, indicating that the liquid always flows into the main or satellite droplet (drainage phenomenon). Though the oscillation of the droplets causes the oscillation of the axial velocity in the filament, the slope of the velocity, i.e., the extension rate, remains constant. The time evolution of the radius of the jet and the first normal stress difference $\phi = \tau_{zz} - \tau_{rr}$ at a fixed position in the filament $z = 3$ is shown in Figs. 6(b) and 6(c), respectively. Clearly, both follow a $1/3\mathrm{De}$ exponential law, not affected by the oscillation in the filament. Thus, we conclude that the oscillation of the droplets has no influence on the thinning characteristic of the filament at large times.

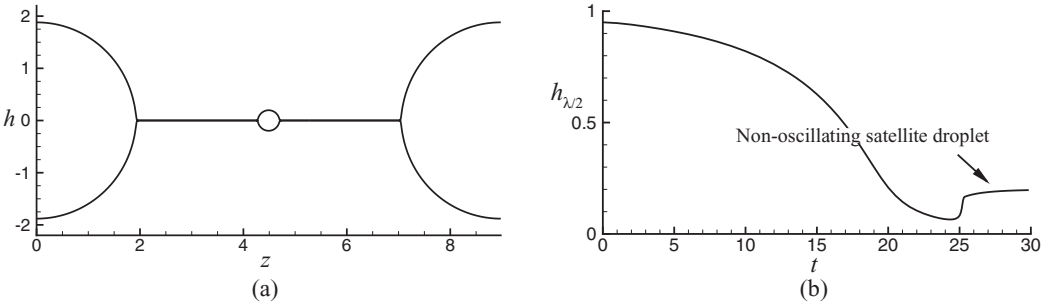

FIG. 7. (a) Typical profile of the beads-on-a-string structure with a non-oscillating satellite droplet between two adjacent main droplets. (b) The time evolution of the radius of the jet at $z = \lambda/2$. $k = 0.7$, Oh $= 0.8$, De $= 0.8$, $\beta = 0.27$.

C. Effects of the axial wave number and the Ohnesorge number on the oscillation of satellite droplets

As shown in Fig. 7, when Oh increases to 0.8 from the value of 0.1 in Fig. 2, the viscoelastic jet evolves into a beads-on-a-string structure with a smaller satellite droplet between two adjacent main droplets, and moreover, the satellite droplet is not oscillating. The size of the satellite droplet increases gradually with time due to drainage, but the system is overdamped and no oscillation takes place. The result reflects the suppression effect of viscosity on the oscillation of the satellite droplet, in agreement with the linear result in Fig. 3 where, for $k = 0.7$ and Oh $= 0.8$, the angular frequency α_i is zero.

Figure 8 illustrates the influence of the axial wave number on the morphology of the jet. When the wave number increases to 0.9 from the value of 0.7 in Fig. 7, a beads-on-a-string structure with no satellite droplet is formed. At small times, the instability of the jet is dominated by the inertial and capillary forces, and the thickness of the filament decreases rapidly. However, at large times, jet breakup is arrested by continuously increasing the elastic force in the filament, and the thickness of the filament decreases slowly following an exponential law, $h_{\lambda/2} \propto \exp(-t/3\mathrm{De})$ [10,12]. Ardekani *et al.* [12] also found that no satellite droplet is formed when the axial wave number is large enough ($k > 0.8$).

To further understand the effects of the axial wave number and viscosity, the situation in the k-Oh plane is shown in Fig. 9, where the solid triangles denote the formation of a beads-on-a-string structure with oscillating satellite droplets, the hollow triangles denote a beads-on-a-string structure with nonoscillating satellite droplets, and the solid squares denote a beads-on-a-string structure with no satellite droplet formed. Clearly, in the k-Oh plane, the region for oscillating satellite droplets is

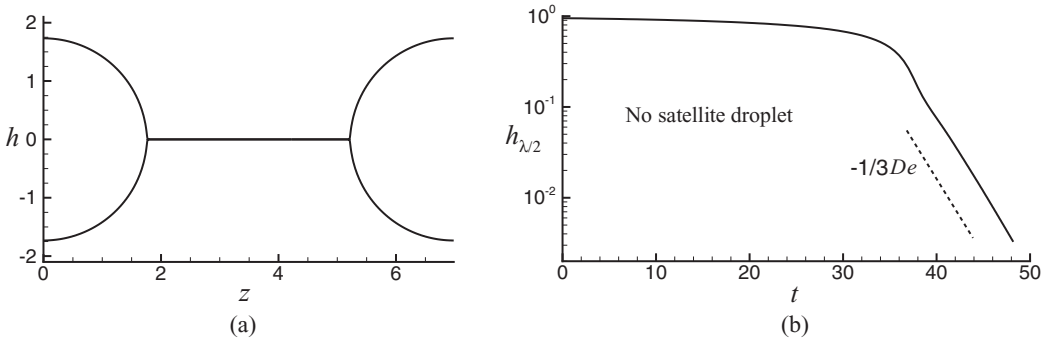

FIG. 8. (a) Typical profile of the beads-on-a-string structure with no satellite droplet generated. (b) The time evolution of the radius of the jet at $z = \lambda/2$. $k = 0.9$, Oh $= 0.8$, De $= 0.8$, $\beta = 0.27$.

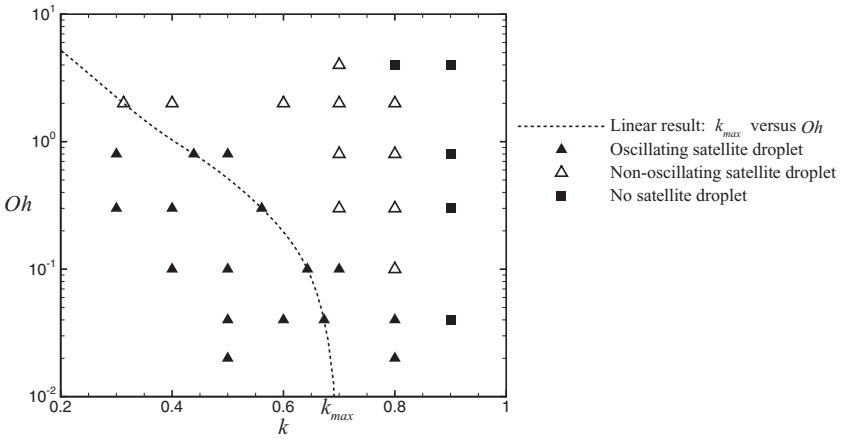

FIG. 9. The effects of the axial wave number k and the Ohnesorge number Oh on the oscillation of a satellite droplet, illustrated in the k-Oh plane. The dashed line is the fitted result of the most unstable wave numbers according to linear theory. De $= 0.8$, $\beta = 0.27$.

located at relatively small axial wave numbers and relatively small Ohnesorge numbers, the region for nonoscillating satellite droplets at relatively large axial wave numbers and relatively large Ohnesorge numbers, and the region for no satellite droplets at sufficiently large axial wave numbers ($k > 0.8$) or sufficiently large Ohnesorge numbers (Oh > 4). At a fixed wave number, as viscosity increases, the oscillation of satellite droplets is damped, the size of satellite droplets is reduced, and eventually the formation of satellite droplets is inhibited. At a fixed Ohnesorge number, oscillating satellite droplets are more easily formed for smaller wave numbers. As the wave number increases, satellite droplets grow smaller, and their oscillation is damped more rapidly, then the oscillation disappears, and finally satellite droplets disappear. For the most unstable wave numbers predicted by linear theory, a beads-on-a-string structure with oscillating satellite droplets develops when Oh < 1.0 and the oscillation of satellite droplets disappears when Oh > 1.0.

D. Effects of the Deborah number on the oscillation of satellite droplets

The effect of the Deborah number on the oscillation of satellite droplets is shown in Fig. 10. For a relatively small axial wave number and Ohnesorge number, as shown in Fig. 10(a), oscillating

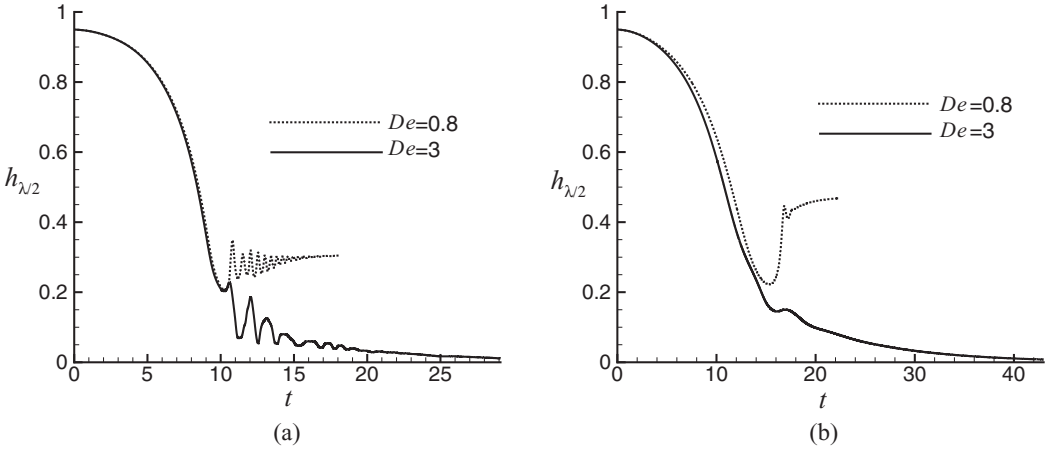

FIG. 10. The time evolution of the radius of the jet at $z = \lambda/2$ for different values of De. (a) $k = 0.6$, Oh $= 0.04$, and (b) $k = 0.8$, Oh $= 0.4$. $\beta = 0.27$.

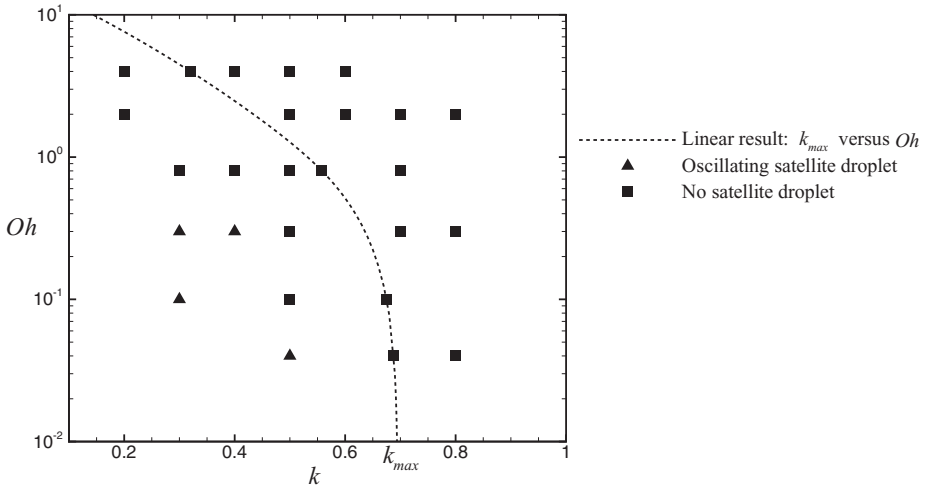

FIG. 11. The situations in the k-Oh plane when De increases to 40. The dashed line is the fitted result of the most unstable wave numbers. $\beta = 0.27$.

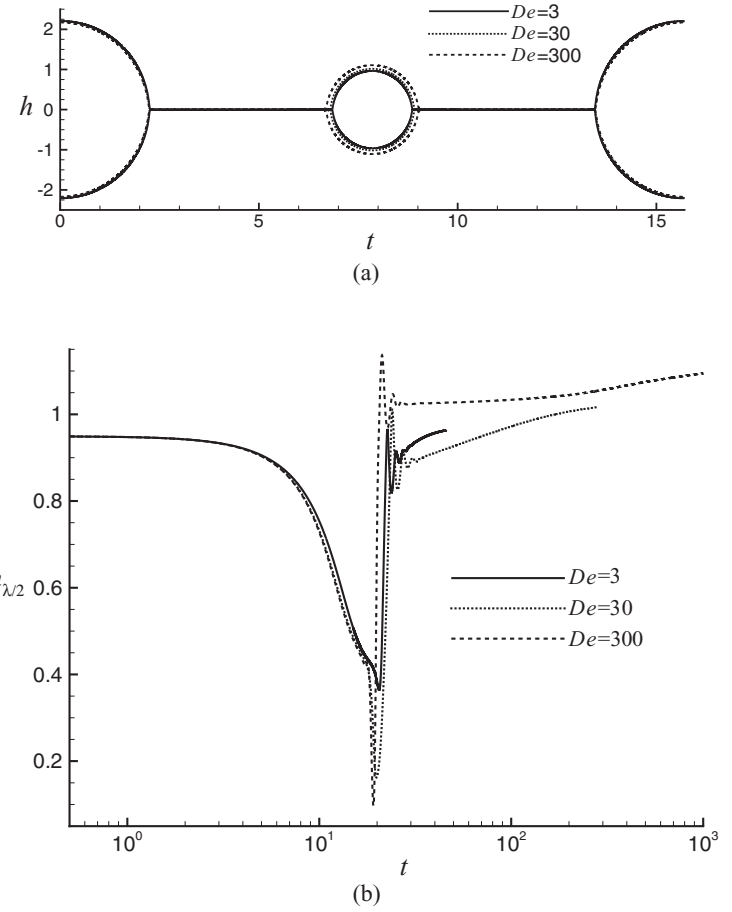

FIG. 12. The situation at small wave numbers. (a) The jet profiles and (b) the time evolution of the radius of the jet at $z = \lambda/2$. $k = 0.4$, Oh $= 0.4$, $\beta = 0.27$.

satellite droplets are formed at a relatively small Deborah number De = 0.8. However, when De increases to 3.0, no permanent satellite droplet is formed ($h_{\lambda/2} \to 0$ at large times), indicating that elasticity suppresses the formation of satellite droplets. In the nonoscillating case shown in Fig. 10(b) where the axial wave number and the Ohnesorge number are relatively large, the formation of satellite droplets is arrested at the larger Deborah number De = 3.

The effect of elasticity is further explored in the k-Oh plane. As can be seen from Fig. 11, when De increases to 40 from the value of 0.8 in Fig. 9, the region in which no satellite droplet is formed is greatly expanded. For the most unstable wave numbers predicted by linear theory, a beads-on-a-string structure with no satellite droplet is formed, different from the case as shown in Fig. 9.

It is another scenario at small wave numbers. As shown in Fig. 12(a) where $k = 0.4$, the size of the satellite droplet slightly increases as De increases, indicating that elasticity cannot suppress the formation of satellite droplets for small wave numbers. Elasticity cannot stop the oscillation of satellite droplets, either. As shown in Fig. 12(b), even when the Deborah number is as large as 300, the satellite droplet is still oscillating. The influence of elasticity on the decay rate of oscillation is also limited.

IV. CONCLUDING REMARKS

The oscillation of satellite droplets in beads-on-a-string structures of Oldroyd-B viscoelastic liquid jets is investigated numerically by using a one-dimensional model. The periods and the decay rates of oscillation estimated from the one-dimensional simulation are compared with the predictions of linear theory. Due to the existence of the filament, the period of oscillation decreases with time, in contrast to linear theory. The axial wave number and viscosity influence greatly the oscillation of satellite droplets. Increasing the axial wave number may lead to the decrease in the period and the increase in the decay rate of oscillation, and increasing viscosity may result in the increase in both the period and the decay rate of oscillation. Elasticity may inhibit the formation of satellite droplets for large wave numbers. For small wave numbers its influence on the oscillation is limited.

In some rheological experiments, it was found that the extensional relaxation time is different from and usually larger than the shear relaxation time [31–33]. That is, the relaxation time is conformation dependent, influenced by the changes in hydrodynamic interactions within and between macromolecular chains. The Oldroyd-B viscoelastic constitutive equation used in this study does not take into account the influence of the conformation on the relaxation time. The other limitation of the present model is that the finite extensibility of polymer chains is ignored and the final stages of the filament thinning cannot be investigated. The effect of finite extensibility and conformation-dependent relaxation times on the oscillation of droplets in a beads-on-a-string structure needs to be explored in the future.

ACKNOWLEDGMENT

The work was supported by the National Natural Science Foundation of China, Grants No. 11272307 and No. 11621202.

[1] M. Goldin, J. Yerushalmi, R. Pfeffer, and R. Shinnar, Breakup of a laminar capillary jet of a viscoelastic fluid, J. Fluid Mech. **38**, 689 (1969).

[2] F. W. Kroesser and S. Middleman, Viscoelastic jet instability, AICHE J. **15**, 383 (1969).

[3] G. Brenn, Z. Liu, and F. Durst, Linear analysis of the temporal instability of axisymmetrical non-Newtonian liquid jets, Int. J. Multiphase Flow **26**, 1621 (2000).

[4] Z. Liu and Z. Liu, Linear analysis of three-dimensional instability of non-Newtonian liquid jets, J. Fluid Mech. **559**, 451 (2006).

[5] Z. Liu and Z. Liu, Instability of a viscoelastic liquid jet with axisymmetric and asymmetric disturbances, Int. J. Multiph. Flow **34**, 42 (2008).
[6] F. Li, X.-Y. Yin, and X.-Z. Yin, Axisymmetric and non-axisymmetric instability of an electrically charged viscoelastic liquid jet, J. Non-Newton. Fluid Mech. **166**, 1024 (2011).
[7] L. J. Yang, M. X. Tong, and Q. F. Fu, Linear stability analysis of a three-dimensional viscoelastic liquid jet surrounded by a swirling air stream, J. Non-Newton. Fluid Mech. **191**, 1 (2013).
[8] H. Chang, E. A. Demekhin, and E. Kalaidin, Iterated stretching of viscoelastic jets, Phys. Fluids **11**, 1717 (1999).
[9] H. J. Shore and G. M. Harrison, The effect of added polymers on the formation of drops ejected from a nozzle, Phys. Fluids **17**, 033104 (2005).
[10] C. Clasen, J. Eggers, M. A. Fontelos, J. Li, and G. H. Mckinley, The beads-on-string structure of viscoelastic threads, J. Fluid Mech. **556**, 283 (2006).
[11] J. Li and M. A. Fontelos, Drop dynamics on the beads-on-string structure for viscoelastic jets: A numerical study, Phys. Fluids **15**, 922 (2003).
[12] A. M. Ardekani, V. Sharma, and G. H. McKinley, Dynamics of bead formation, filament thinning and breakup in weakly viscoelastic jets, J. Fluid Mech. **665**, 46 (2010).
[13] P. P. Bhat, S. Appathurai, M. T. Harris, and O. A. Basaran, On self-similarity in the drop-filament corner region formed during pinch-off of viscoelastic fluid threads, Phys. Fluids **24**, 083101 (2012).
[14] M. Renardy, A numerical study of the asymptotic evolution and breakup of Newtonian and viscoelastic jets, J. Non-Newton. Fluid Mech. **59**, 267 (1995).
[15] V. M. Entov and E. J. Hinch, Effect of a spectrum of relaxation times on the capillary thinning of a filament of elastic liquid, J. Non-Newton. Fluid Mech. **72**, 31 (1997).
[16] R. Sattler, S. Gier, J. Eggers, and C. Wagner, The final stages of capillary break-up of polymer solutions, Phys. Fluids **24**, 023101 (2012).
[17] J. Eggers, Instability of a polymeric thread, Phys. Fluids **26**, 033106 (2014).
[18] D. F. James, Boger Fluids, Annu. Rev. Fluid Mech. **41**, 129 (2009).
[19] D. T. Papageorgiou, On the breakup of viscous-liquid threads, Phys. Fluids **7**, 1529 (1995).
[20] F. Li, X. Y. Yin, and X. Z. Yin, One-dimensional nonlinear instability study of a slightly viscoelastic, perfectly conducting liquid jet under a radial electric field, Phys. Fluids **28**, 053103 (2016).
[21] L. Rayleigh, On the instability of jets, Proc. London Math. Soc. **10**, 4 (1878).
[22] L. Rayleigh, On the capillary phenomena of jets, Proc. R. Soc. London A **29**, 71 (1879).
[23] S. Middleman, Stability of a viscoelastic jet, Chem. Eng. Sci. **20**, 1037 (1965).
[24] H. F. Bauer, Surface- and interface oscillations in an immiscible spherical visco-elastic system, Acta Mech. **56**, 127 (1985).
[25] H. F. Bauer and W. Eidel, Vibration of a viscoelastic spherical immiscible liquid-system, Z. Angew. Math. Mech. **67**, 525 (1987).
[26] D. B. Khismatullin and A. Nadim, Shape oscillations of a viscoelastic drop, Phys. Rev. E **63**, 061508 (2001).
[27] G. Brenn and S. Teichtmeister, Linear shape oscillations and polymeric time scales of viscoelastic drops, J. Fluid Mech. **733**, 504 (2013).
[28] L. Yang *et al.*, Determination of dynamic surface tension and viscosity of non-Newtonian fluids from drop oscillations, Phys. Fluids **26**, 113103 (2014).
[29] H. Lamb, On the oscillations of a viscous spheroid, Proc. Lond. Math. Soc. **13**, 51 (1881).
[30] A. Prosperetti, Free oscillations of drops and bubbles: The initial-value problem, J. Fluid Mech. **100**, 333 (1980).
[31] C. Clasen *et al.*, How dilute are dilute solutions in extensional flows? J. Rheol. **50**, 849 (2006).
[32] J. Dinic, Y. Zhang, L. N. Jimenez, and V. Sharma, Extensional relaxation times of dilute, aqueous polymer solutions, ACS Macro Lett. **4**, 804 (2015).
[33] R. Prabhakar, S. Gadkari, T. Gopesh, and M. J. Shaw, Influence of stretching induced self-concentration and self-dilution on coil-stretch hysteresis and capillary thinning of unentangled polymer solutions, J. Rheol. **60**, 345 (2016).